

MATERIAL PROPERTIES OF TETRIX FOR DEMONSTRATION EQUIPMENT

YU YAMADA¹, RYOSUKE SUZUKI¹, KAITO YOSHINAGA², TAKAAKI SUZUKI¹
MASAAKI MATSUBARA¹ AND KOU YAMADA¹

¹Graduate School of Science and Technology

²School of Science and Technology
Gunma University

1-5-1 Tenjincho, Kiryu 376-8515, Japan

{t161b602; r_suzuki; suzuki.taka; m.matsubara; yamada; t14302118}@gunma-u.ac.jp

Received May 2017; revised August 2017

ABSTRACT. *TETRIX is the expansion kit for LEGO MindStorms and includes powerful motors, a battery, and high-strength aluminum alloy components. TETRIX and LEGO MindStorms have the potential of producing demonstration equipment easily. In this paper, we carry out a three-point bending test to determine the strength of the U-shaped aluminum alloy channel in TETRIX and to demonstrate the effectiveness of TETRIX from the viewpoint of the strength of the components. In addition, we produce a cushion robot made from TETRIX components that can carry a person and evaluate the safety of this robot. The U-shaped channel has two kinds of ultimate bending strength depending on loading direction. The ultimate bending strengths of the channel subjected to load from vertical and horizontal directions are about 180[MPa] and 50[MPa], respectively. The TETRIX components have adequate strength for demonstration equipment, although the loading direction should also be considered in the design process. The carrying capacity of the cushion robot is 159[kg]. The cushion robot has adequate carrying capacity and strength to carry a person safely. Therefore, TETRIX has excellent potential for demonstration equipment.*

Keywords: LEGO MindStorms, TETRIX, Equipment development, Bending strength, Aluminum alloy, Safety

1. Introduction. In this paper, we focus on LEGO MindStorms and TETRIX as a tool that can produce a robot and a piece of equipment. LEGO MindStorms is robotics educational material that the LEGO Company started to sell in 1998. LEGO blocks made of ABS resin are included in LEGO MindStorms, and can assemble the robot and the equipment inexpensively, quickly, and easily. Many LEGO blocks, two types of motors, and various kinds of sensors, such as a color sensor, an ultrasonic sensor, a touch sensor, a gyro sensor, and an infrared sensor, are included in LEGO MindStorms. In addition, software is included to easily create control programs of motors and sensors in LEGO MindStorms without knowledge of programming languages. LEGO MindStorms is very useful for experimental equipment for the study of the automatic control of an intelligent robot. Therefore, LEGO MindStorms is widely used in educational institutions from the elementary school to university. LEGO MindStorms is also widely used as equipment material [1, 2, 3]. For example, the handstand pendulum [4] that can be a controlled servo system was produced from LEGO MindStorms.

However, LEGO blocks made of ABS resin are so weak that the blocks cannot be used for intelligent locomotion robots that could carry a person. Robots that are able to carry a person can be produced by using TETRIX, the expansion kit of LEGO MindStorms,

which includes high-strength aluminum alloy components, powerful motors, and gears. Thus, various kinds of equipment can be produced quickly by using TETRIX.

Various kinds of robots have been developed, such as industrial robots [5], life-support robots [6], and nursing care robots [7]. These robots are already essential for daily life. Recently, intelligent robots, such as an autonomous driving car [8], have become the focus of attention and many theoretical and experimental studies of these robots have been performed. Intelligent robots have many sensors and can self-judge and move. The use of an intelligent wheelchair system was reported in [9]. It can provide easy control of locomotion devices for the disabled and senior citizens. However, in order to study and develop intelligent robots, demonstration equipment is needed. In experimental studies on intelligent robots, small-scale demonstration equipment is used as a first step. For example, an autonomous formula racing car was produced in [10]. Because significant costs and efforts were needed to produce this racing car of a size that can carry a person, TETRIX could be used as the material for small-scale demonstration equipment that could carry a person to study intelligent robots.

The inadequate strength of demonstration equipment may cause a serious accident that endangers people. To produce safe and secure demonstration equipment, adequate design is required. However, the LEGO Company has not released the TETRIX strength data required for adequate design. The strength and deformation behavior of TETRIX must be adequately understood to assure the safety of the person using the demonstration equipment during an experiment.

In this paper, three-point bending tests were carried out to investigate the strength and deformation behavior of a U-shaped aluminum alloy component of TETRIX. In addition, the demonstration equipment that could carry a person was actually produced, and the safety of the equipment was verified from the viewpoint of material mechanics based on the strength data of the U-shaped component.

The remainder of the paper is organized as follows. In Section 2, the bending strength and deformation behavior of the U-shaped channel are clarified. In Section 3, the demonstration equipment is produced and the structural strength of the equipment is discussed and evaluated based on the strength of the parts such as the wheels and the U-shaped channel. Section 4 concludes.

2. Experiment on Bending Strength of Aluminum Alloy Components.

2.1. Experimental method. U-shaped channels made of A7005 aluminum alloy were prepared as specimens. Photograph of the specimen is shown in Figure 1.

The U-shaped channel has good potential for a main frame of the demonstration equipment, which is subjected to bending, because the channel has a large section modulus.



FIGURE 1. U-shaped channel

The specimen has two kinds of holes with different diameters, $\phi 7.9[\text{mm}]$ and $\phi 3.7[\text{mm}]$, which are regularly arranged on it. A schematic illustration of the specimen geometry is shown in Figure 2 and the specimen dimensions are listed in Table 1. Here, L_s , H_s , B_s , and t_s show depth, height, width, and thickness of the U-shaped channel, respectively. The terms h_s and b_s are expressed as

$$h_s = H_s - t_s. \tag{1}$$

$$b_s = B_s - 2t_s. \tag{2}$$

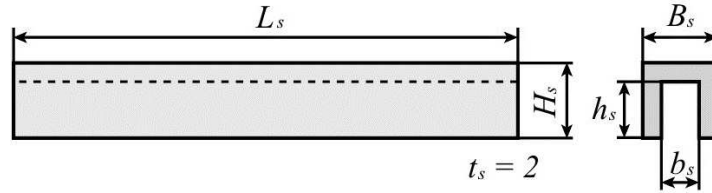


FIGURE 2. Schematic illustration of U-shaped channel

TABLE 1. The sizes of U-shaped channel

L_s [mm]	H_s [mm]	B_s [mm]	h_s [mm]	b_s [mm]	t_s [mm]
288	32	32	30	28	2

To determine the strength of the U-shaped channel, three-point bending tests were carried out on the specimens using a universal testing machine (Saginomiya, $UH - 100[\text{kN}]$) according to ISO 7438:2005. A schematic illustration of the three-point bending test is shown in Figure 3. In the bending test, the specimen was placed on two lower supports, and was then pushed and bent by the punch.

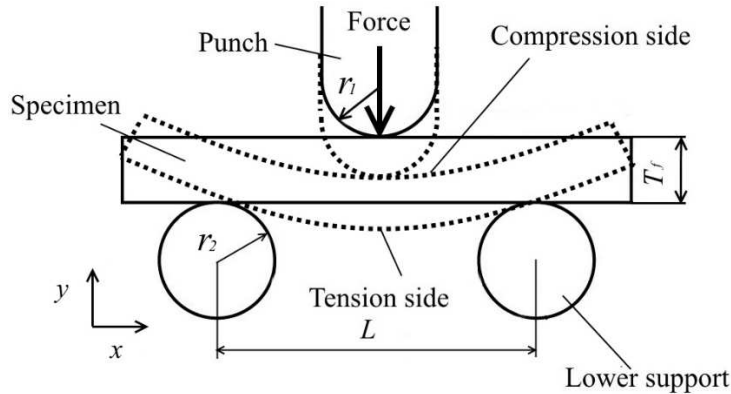


FIGURE 3. Schematic illustration of three-point bending test

The support span L is defined by ISO 7438:2005 as the next equation.

$$L = 2r_1 + 3T_f. \tag{3}$$

Here, the punch radius and the support radius were $r_1 = r_2 = 15[\text{mm}]$, and the height of specimen $T_f = 32[\text{mm}]$. In this paper, support span L was $126[\text{mm}]$. The upper and lower sides of the specimen were subjected to compressive and tensile stresses caused by

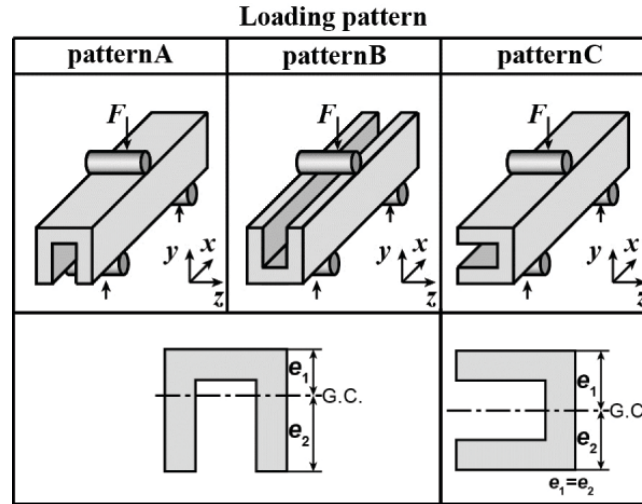


FIGURE 4. Schematic illustrations of loading directions

bending load, respectively. Three types of bending tests with different loading direction were carried out as shown in Figure 4. All bending tests were carried out under a constant cross head speed 0.5[mm/min]. All types of the bending tests were performed three times to confirm the repeatability. The sampling frequency of both the applied load, F , and stroke, y , was 2[Hz]. The maximum bending stress σ occurs at the center in x -direction of the specimen. The maximum bending stress is expressed as,

$$\sigma = \frac{M}{Z}. \quad (4)$$

Here, the bending moment M at the center in x -direction of the specimen is expressed as,

$$M = \frac{FL}{4}. \quad (5)$$

The section modulus Z is a geometric property for a given cross section area and is a function of y . Both section moduli for the lower and upper sides of the specimen should be calculated, because the maximum tensile and compressive bending stresses occur at the lower and the upper sides, respectively. The section modulus is expressed as,

$$Z = \frac{I}{e}, \quad (6)$$

where I is the moment of inertia of the area and e is the distance from neutral axis of the specimen to the upper or lower side of the specimen. The second moment of area I is calculated by next equation.

$$I = \frac{B_s e_1^3 - b_s h^3 + 2t_s e_2^3}{3}, \quad (7)$$

for loading patterns A and B, and

$$I = \frac{H_s B_s^3 - (e_1 - t_s) b_s^3}{12}, \quad (8)$$

for loading pattern C.

e_1 and e_2 are calculated by the equation

$$e_1 = \frac{2t_s H_s^2 + b_s t_s^2}{2(2t_s H_s + b_s t_s)}, \quad (9)$$

$$e_2 = H_s - e_1, \tag{10}$$

for loading patterns A and B, and

$$e_1 = e_2 \tag{11}$$

$$= \frac{B_s}{2}, \tag{12}$$

for loading pattern C.

The bending strain ε of the specimen is calculated according to ISO 178:2010 by the equation

$$\varepsilon = \frac{600sT_f}{L^2}. \tag{13}$$

Here, s is the deflection of the center in the x -direction of the specimen and is considered to be equal to y . The bending stress was plotted against the bending strain and the linear limit stress σ_k , 0.2% proof stress, $\sigma_{0.2}$, and the maximum stress, σ_u , were obtained.

In addition, to discuss the breaking behavior of the U-shaped channel, the specimen was filmed with a video camera during the bending test.

2.2. Result of strength of the U-shaped channel. The bending stress-bending strain curves of loading patterns A, B, and C are shown in Figure 5, Figure 6, and Figure 7, respectively. The bending stresses of the upper and lower sides of the specimen are plotted in these figures. The bending stress-bending strain curve of loading pattern A is very similar to loading pattern B. Good repeatability was observed for loading patterns A and B. On the other hand, the bending stress of loading pattern C was lower than or equal to those of loading patterns A and B. On the loading pattern C Figure 7, one bending stress is over two times higher than that of other two bending stresses. We considered this high bending stress as error data.

The mean maximum load of all the patterns became approximately the same. This result indicated that a slim column subjected to compressive load buckled only for loading pattern C as shown in Figure 8. Photographs of the broken specimens of all the loading patterns are shown in Figure 9. The specimen of loading pattern C broke only in buckling at the slim column.

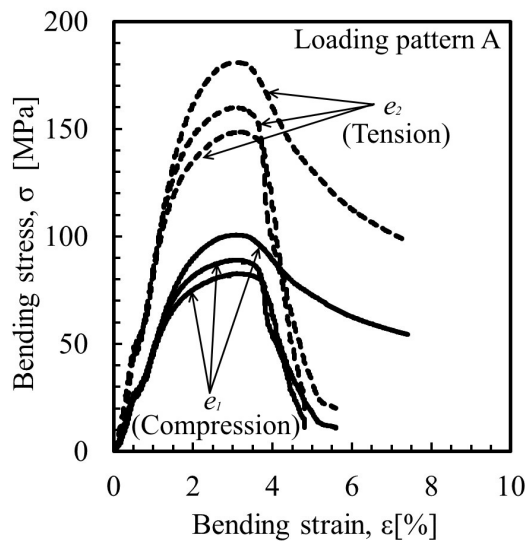


FIGURE 5. Bending stress-bending strain curve for loading pattern A

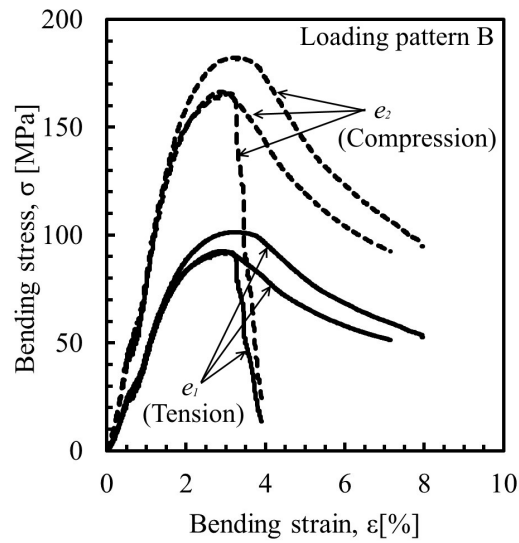


FIGURE 6. Bending stress-bending strain curve for loading pattern B

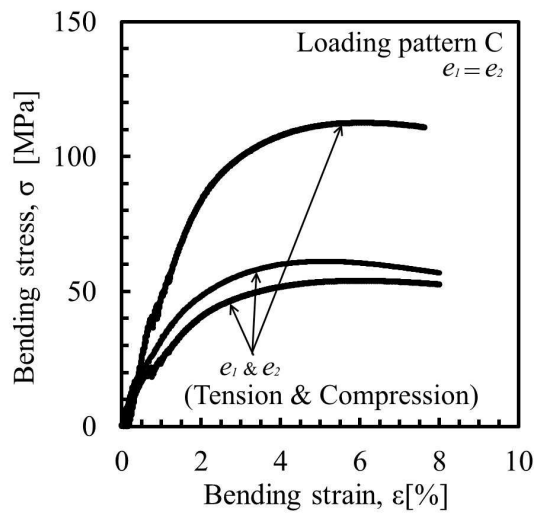


FIGURE 7. Bending stress-bending strain curve for loading pattern C

TABLE 2. Mean linear limit stress, mean 0.2% proof stress, and mean ultimate bending strength

Loading pattern	σ_k [MPa]	$\sigma_{0.2}$ [MPa]	σ_u [MPa]
A[e_1]	27	68	91
A[e_2]	48	129	163
B[e_1]	27	82	95
B[e_2]	49	144	171
C[e_1]	26	35	78

In the case of loading pattern A, the crack can be observed around the hole near the e_2 side subjected to tensile stress (Figure 9(a)). However, for loading pattern B, the crack cannot be observed around the hole near the e_1 side (Figure 9(c) and Figure 9(d)), although the e_1 side of the specimen was subjected to tensile stress. In addition, a large deformation was observed on the e_2 side that was subjected to compressive stress for

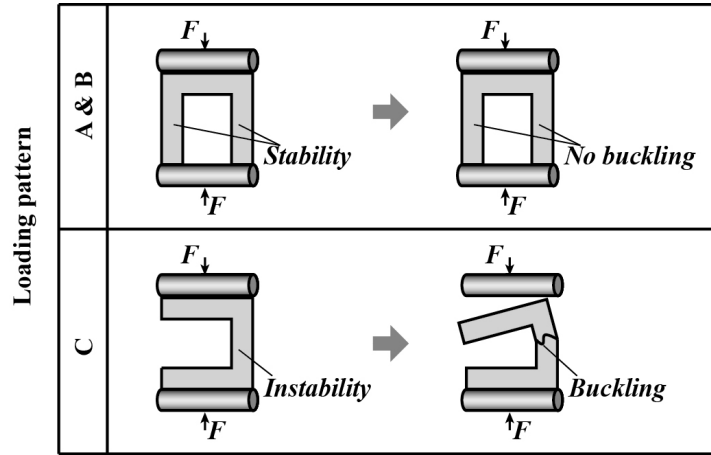


FIGURE 8. Schematic illustration of the buckling of the U-type channel

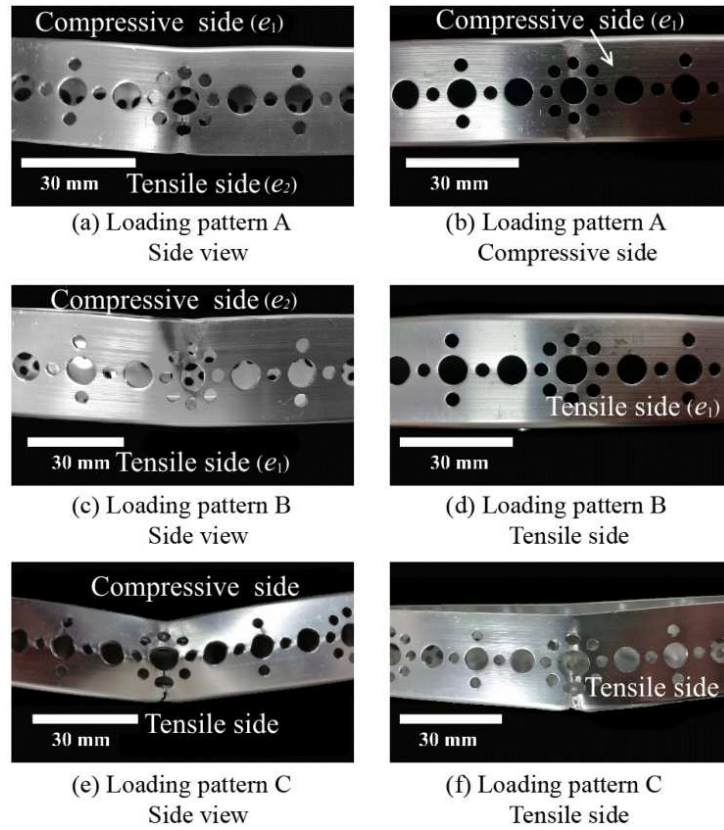


FIGURE 9. Photographs of the broken specimens for all loading patterns

TABLE 3. Mean maximum force

Loading pattern	A	B	C
Maximum force	4966	5214	5199

loading pattern B. Therefore, in both loading patterns A and B, the U-type TETRIX channel was broken from the open side because the applied stress on the open side was higher than that on the closed side. The specimen buckled at the slim column for loading pattern C (Figure 9(e)). In addition, for loading pattern C, the crack was observed on

the tensile side because the large plastic deformation caused by buckling led to cracking around the hole on the tensile side (Figure 9(f)).

Generally, the 0.2% proof stress or the ultimate strength is used for design purposes. The slope of the bending stress-bending strain curve changes at a bending strain of about $\varepsilon = 0.5$ to 1[%] for all loading patterns. This result indicated that the plastic deformation started at this bending strain, although this bending strain appears to be in the elastic region. Thus, the linear limit stress, σ_k , is defined as the bending stress at this bending strain. The 0.2% proof stress, $\sigma_{0.2}$, is defined as the stress at which 0.2[%] strain remained after unloading. The ultimate bending strength, σ_u , is the maximum stress of the bending stress-bending strain curve. The 0.2% proof stress obtained experimentally ranged from 43[MPa] to 144[MPa] and the ultimate bending strength ranged from 91[MPa] to 171[MPa]. In previous studies ([11] and [12]), the 0.2% proof stress of the A7005 aluminum alloy ranged from 213[MPa] to 501[MPa] and the ultimate tensile strength from 325[MPa] to 561[MPa]. The present 0.2% proof stress and ultimate bending stress were significantly lower than those in these reports, because in the present specimens, buckling and stress concentration occur. Buckling occurs when a straight slim column that is subjected to axial compression suddenly undergoes bending. The stress concentration factor of the circular hole end in an infinite flat plate is 3. The stress that occurs in a plate with a circular hole is three times higher than that of the plate without a circular hole.

2.3. Breaking behavior of the U-shaped channel. The bending stress-time curve of loading pattern A is shown in Figure 10, together with photographs of the specimen during the bending test.

The solid line shows the stress of the e_1 side and the broken line that of the e_2 side. The elastic slope changes in 16[s] to 26[s]. However, the macroscopic plastic deformation of the specimen is not observed in the photographs of 16[s] to 26[s] of Figure 10. The

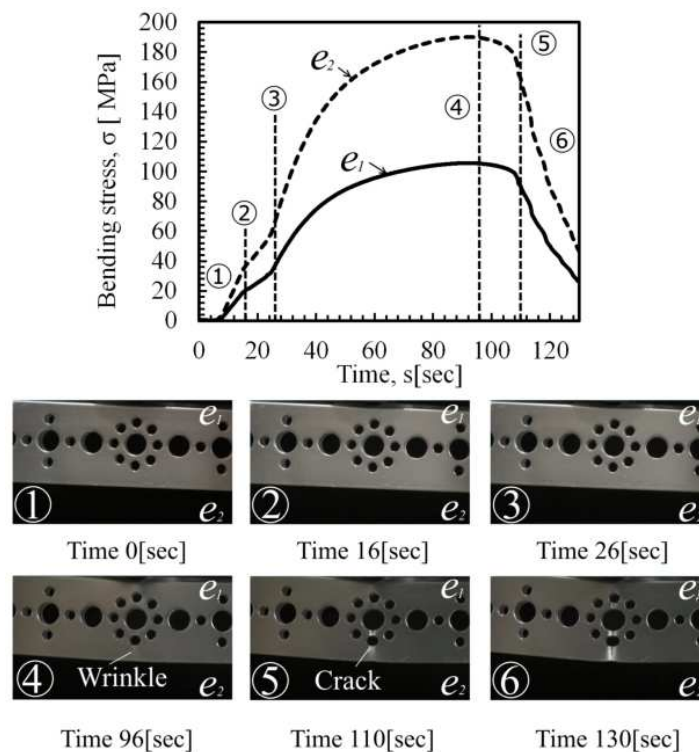


FIGURE 10. Bending stress-time curve and photographs of the shape change of the broken specimens with time

e_2 side of the specimen wrinkles at the ultimate bending stress (96[s]), and the bending stress rapidly decreases at 110[s] because the crack penetrates the material of the e_2 side. Finally, the specimen is broken after 130[s].

3. Production and Strength Evaluation of a Transfer Robot for a Person.

3.1. Production of a cushion robot as a transfer robot. To demonstrate that a device constructed of TETRIX components is effective as experimental equipment for the study of an automatic control field, we produced a cushion robot that could automatically carry a person in any direction without turning. The cushion robot can be used as demonstration equipment for our autonomous running control theory. In order for the cushion robot to move in any direction, we adapted a mecanum wheel that was used in a previous study [13]. Four 50[mm]-wide mecanum wheels with 100[mm] diameter were installed on the cushion robot to enable sensitive control. The six support wheels were also installed on the cushion robot to improve the carrying capacity. The limit loads of the mecanum wheel and the support wheel were 15[kg] and 30[kg], respectively. Thus, the carrying capacity of the cushion robot was calculated at 240[kg] based on the wheel strength. The cushion robot was equipped with a LEGO MindStorms infrared sensor. An operator could control the cushion robot using an infrared beacon.

A photograph of the cushion robot is shown in Figure 11. The cushion robot was about 600[mm] in width, 500[mm] in depth, and 300[mm] in height. A wooden board was installed on the framework with the wheels, the motors, and the sensors. A cushion was placed on the wooden board as a seat. A photograph of the framework of the cushion robot is shown in Figure 12. The framework of the cushion robot consisted of 13 U-type aluminum channels, four mecanum wheels, six support wheels, two motors, and an infrared sensor. The U-type channels were fixed with bolts and nuts. The cushion robot could not only be controlled by an operator but also moved automatically using line trace control [14] and/or obstacle recognition [15].

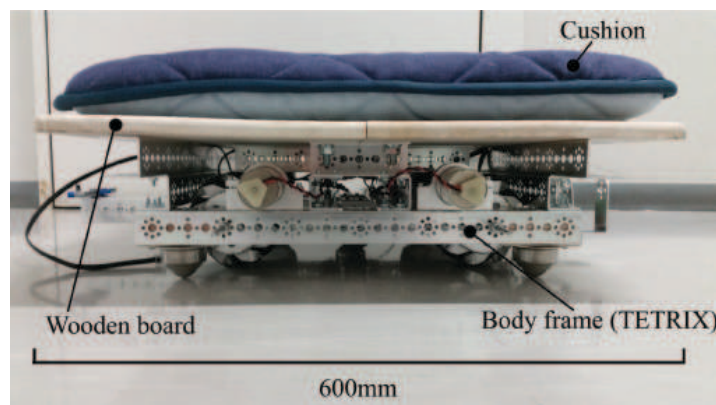


FIGURE 11. Photograph of the cushion robot

3.2. Strength evaluation of the cushion robot. The cushion robot received two loads of bending stress and compressive stress. Generally, the bending strength is weaker than compressive strength. Therefore, only the bending strength was calculated in this experiment. The carrying capacity of the cushion robot was calculated based on the wheel strength, but the strength of the U-shaped channel was not considered. The load capacity of the cushion robot should be considered from the bending strength of the channel. The maximum stress applied on the channel was calculated and compared with the bending

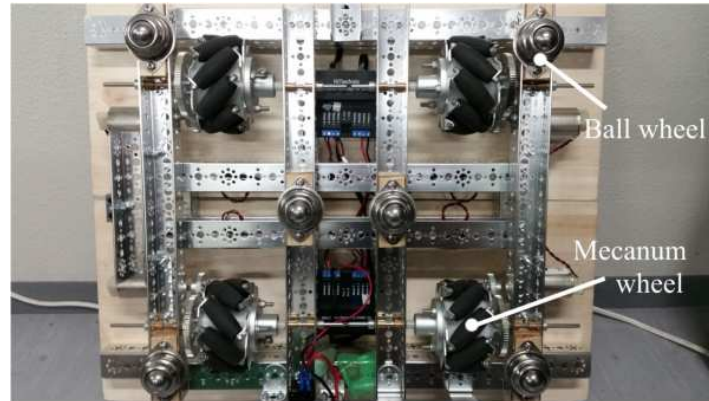


FIGURE 12. Photograph of the framework of the cushion robot

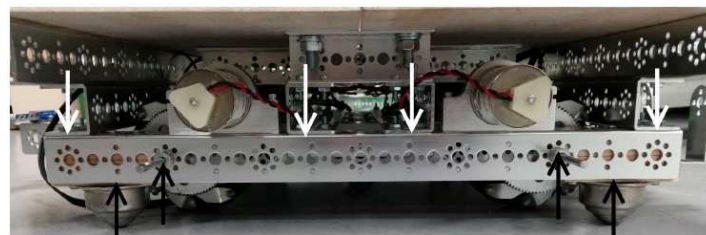


FIGURE 13. Aluminum channel A subjected to a bending load in the body frame of the cushion robot

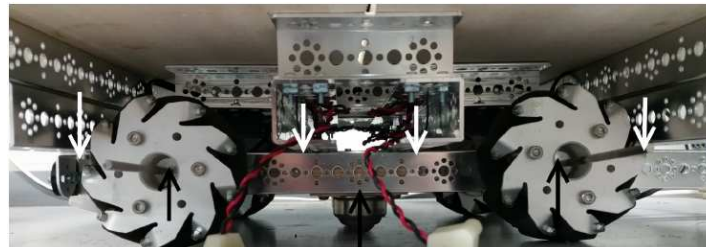


FIGURE 14. Aluminum channel B subjected to a bending load in the body frame of the cushion robot

strength of the channel to provide adequate evidence of the safety of the cushion robot. In addition, we discussed the potential of the TETRIX material for experimental equipment for the study of an automatic control field from the viewpoint of the strength of the U-shaped channel and of safety.

The safety of the cushion robot is discussed from the viewpoint of the strength of the TETRIX aluminum components. The U-type aluminum channels subjected to bending stress form only two parts in the framework of the cushion robot. The other aluminum channels are mainly subjected to compressive stress. Two kinds of the aluminum channels subjected to bending stress are shown in Figure 13 and Figure 14. The maximum bending stress applied to the channel was calculated and the safety of the cushion robot discussed. To calculate the applied maximum bending stress, the aluminum channels were simplified to be statically indeterminate beams as shown in Figure 15 and Figure 16. Aluminum channel A (Figure 13 and Figure 15) is subjected to transverse load from four points and is supported by three wheels. Aluminum channel B (Figure 14 and Figure 16) is subjected to transverse load from four points and is supported by four wheels. For aluminum channels

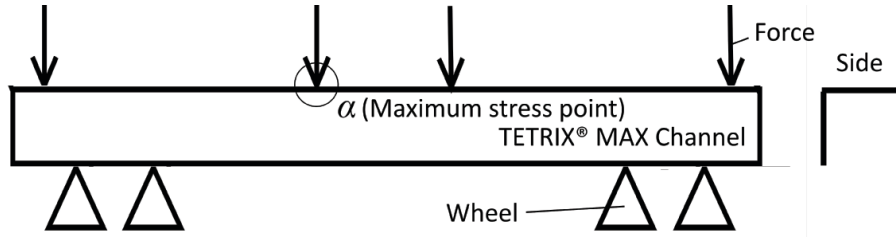


FIGURE 15. Simplification of aluminum channel A subjected to a bending load

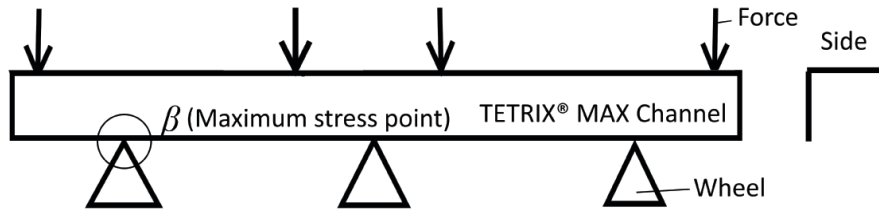


FIGURE 16. Simplification of aluminum channel B subjected to a bending load

A and B, the applied maximum bending stress occurred at points α (Figure 15) and β (Figure 16), respectively. The applied maximum bending stresses at points α and β were calculated to be 2.46[MPa] and 3.40[MPa], respectively, assuming that the weight of the occupant is 60[kg]. The applied maximum bending stresses were lower than the linear limit strength of the aluminum channel. Therefore, the cushion robot is safe from the viewpoint of the strength of the aluminum channel. Aluminum channels A and B could respectively support 220[kg] and 159[kg] assuming a safety factor of 3 when the linear limit strength is used as the reference strength. The safety factor is the safety margin and the reference strength is the strength used in the design. The cushion robot had a maximum safe carrying capacity of 159[kg]. The TETRIX aluminum channels had adequate strength as the material for demonstration equipment for the study of the automatic control of an intelligent robot. Therefore, TETRIX has excellent potential for such purpose.

4. Conclusions. In this paper, the aim was to investigate the safety of demonstration equipment made of TETRIX components and its ability to carry a person to verify the control theory. Three-point bending tests were carried out to investigate the strength of TETRIX, given that LEGO MindStorms does not release the strength data, despite being indispensable for adequate strength design of demonstration equipment. The bending strength of a TETRIX U-shaped aluminum alloy component was about 27[MPa] regardless of the loading pattern.

The U-shaped component was broken by cracking occurring from the open side in loading patterns A and B. In loading pattern C, the component was broken by buckling of the side wall.

As demonstration equipment for the verification of the control theory, the cushion robot could be designed and produced considering the strength of the U-shaped component. The maximum carrying capacity of the cushion robot was 159[kg], which is more than twice the average weight of a Japanese adult male (70[kg]). Therefore, the cushion robot can be safely used for verification of the control theory from the viewpoint of carrying capacity.

The strength criteria could be obtained for adequate design of demonstration equipment. Safe demonstration equipment for verification of the control theory can be produced by using TETRIX, inexpensively, easily and quickly.

The TETRIX aluminum channel has adequate strength as a material for demonstration equipment for the study of the automatic control of an intelligent robot. Therefore, TETRIX has excellent potential for such a purpose.

REFERENCES

- [1] P. J. Bradley, J. A. Puente, J. Zamorano and D. Brosnan, A platform for real-time control education with LEGO MINDSTORMS, *The 9th IFAC Symposium Advances in Control Education*, vol.45, pp.112-117, 2012.
- [2] K. Houda and R. Lakel, Synchronized communication in a set of autonomous mobile robots using Bluetooth technology, *Procedia Computer Science*, vol.73, pp.154-161, 2015.
- [3] S. A. Fillippov, A. L. Fradkov, I. V. Ashikhmina and R. E. Seifullaev, LEGO mindstorms NXT robots and oscillators in control education, *IFAC Proceedings Volumes*, vol.43, pp.156-160, 2010.
- [4] R. E. Seifullaev, Speed gradient energy and sampled-data control of cart-pendulum system, *The 9th IFAC Symposium Advances in Control Education*, vol.45, pp.478-483, 2012.
- [5] F. Leutert and K. Schilling, Augmented reality for telemaintenance and -inspection in force-sensitive industrial robot applications, *The 2nd IFAC Conference on Embedded Systems, Computer Intelligence and Telematics (CESCIT 2015)*, vol.48, pp.153-158, 2015.
- [6] R. Borja, J. R. de la Pinta, A. Álvarez and J. M. Maestre, Integration of service robots in the smart home by means of UPnP: A surveillance robot case study, *Robotics and Autonomous Systems*, vol.61, pp.153-160, 2013.
- [7] D. Fischinger, P. Einramhof, K. Papoutsakis, W. Wohlkinger, P. Mayer, P. Panek, S. Hofmann, T. Koertner, A. Weiss, A. Argyros and M. Vincze, Hobbit, a care robot supporting independent living at home: First prototype and lessons learned, *Robotics and Autonomous Systems*, vol.75, pp.60-78, 2016.
- [8] E. Drozdova, S. Hopfgarten, E. Lazutkin and P. Li, Autonomous driving of a mobile robot using a combined multiple-shooting and collocation method, *The 9th IFAC Symposium on Intelligent Autonomous Vehicles (IAV 2016)*, vol.49, pp.193-198, 2016.
- [9] F. Pasteau, V. K. Narayanan, M. Babel and F. Chaumette, A visual servoing approach for autonomous corridor following and doorway passing in a wheelchair, *Robotics and Autonomous Systems*, vol.75, pp.28-40, 2016.
- [10] J. Ni and J. Hu, Dynamics control of autonomous vehicle at driving limits and experiment on an autonomous formula racing car, *Mechanical Systems and Signal Processing*, vol.90, pp.154-174, 2017.
- [11] T. S. Shih and Q. Y. Chung, Fatigue of as-extruded 7005 aluminum alloy, *Materials Science and Engineering: A*, vol.348, pp.333-344, 2003.
- [12] T. Zhao and Y. Jiang, Fatigue of 7075-T651 aluminum alloy, *International Journal of Fatigue*, vol.30, pp.834-849, 2008.
- [13] O. Diegel, A. Badve, G. Bright, J. Potgieter and S. Tlate, Improved mechanism wheel design for omni-directional robots, *Proc. of Australasian Conference on Robotics and Automation*, pp.117-121, 2002.
- [14] A. A. Kapitonov, A. A. Bobtsov, Y. A. Kapitanyuk, D. S. Sysolyatin, E. S. Antonov, A. A. Pyrkin and S. A. Chepinskiy, Course of lab activities on control theory based on the LEGO NXT, *The 19th IFAC World Congress*, vol.47, pp.9063-9068, 2014.
- [15] A. A. Bobtsov, A. A. Pyrkin, S. A. Kolyubin, A. A. Kapitonov, A. D. Feskov, S. M. Vlasov, A. Y. Krasnov, A. V. Khovanskiy and S. V. Shavetov, LEGO mindstorms NXT for students' research projects in control field, *The 9th IFAC Symposium on Advances in Control Education*, vol.45, pp.102-106, 2012.